JOURNAL OF GUIDANCE, CONTROL, AND DYNAMICS
Vol. 30, No. 6, November–December 2007

Modeling, Analysis, and Simulation of GPS Carrier Phase for Spacecraft Relative Navigation

Mark L. Psiaki* and Shan Mohiuddin†
Cornell University, Ithaca, New York 14853-7501

DOI: 10.2514/1.29534

Models of Global Positioning System carrier-phase measurements have been derived, analyzed, and used to develop an offline simulator. This work is being carried out to support the development of carrier-phase differential Global Positioning System methods for relative navigation of formations of spacecraft that orbit in geosynchronous Earth orbit and high-altitude Earth orbit. Carrier-phase models are built up by considering signal generation on the Global Positioning System satellite and signal processing in the user receiver. An analysis of measured carrier-phase has been used to develop receiver design guidelines which guarantee that a receiver's outputs can be used by carrier-phase differential Global Positioning System algorithms that resolve carrier-phase ambiguities as exact integers. The carrier-phase simulation includes errors such as incorrect Global Positioning System ephemerides, thermal noise, multipath, circular-polarization-induced phase windup, and altitude-dependent ionospheric delay. Simulation results demonstrate the efficacy and limitations of carrier-phase differential Global Positioning System methods for use in relative navigation of spacecraft formations.

I. Introduction

CARRIER-PHASE differential Global Positioning System (CDGPS) techniques are being developed to do centimeter-level relative position estimation for Earth-orbiting spacecraft formations. Spacecraft formations are of interest because they can yield improved performance for a variety of mission objectives which include probing the Earth's magnetosphere, study of celestial objects using optical interferometry, and monitoring of activities on the Earth using radar interferometry [1].

A number of researchers have studied the use of CDGPS techniques for relative position determination in low-Earth orbit (LEO) [2–5], but little has been done for higher orbits. The use of GPS at altitudes above about 3000 km becomes difficult because a user receiver will lie outside of the main lobes of more and more GPS transmitter antennas as its altitude increases above this limit. Recent work, however, has demonstrated the feasibility of acquiring and tracking weak GPS side-lobe signals at altitudes ranging up to geosynchronous Earth orbit (GEO) and beyond to high-altitude Earth orbit (HEO) [6–8]. This work has sparked an interest in the possibility of using CDGPS for relative navigation of formations at these altitudes.

The present work develops tools for performing analytical and simulation studies of the feasibility and performance of high-altitude CDGPS systems. These tools include a signal model, design guidelines for appropriate receivers, and offline simulation techniques. They are slated to be used to guide the design of estimation algorithms and receivers for use in hardware-in-the-loop simulation studies and flight experiments.

One question of particular interest concerns whether carrier-phase ambiguities can be resolved as integer numbers of cycles when performing relative navigation in GEO and HEO. The resolution of ambiguities as integers instead of real numbers would provide a gain in accuracy that could offset losses due to poor constellation geometry and decreased signal-to-noise ratio. Therefore, it is important to answer the question of how and when carrier-phase ambiguities can be resolved as integers.

This paper's developments draw on various areas of GPS expertise. CDGPS techniques are highly developed in the surveying and geodesy communities, and works such as [9–11] provide valuable insights into the modeling and processing of CDGPS measurements. Additional helpful material for simulating GPS signals received by orbiting spacecraft is contained in [12].

This paper makes four main contributions. First, it develops a high-fidelity carrier-phase measurement model that can be used in simulators, receivers, and CDGPS relative navigation estimators. This model is used to resolve the question of when carrier-phase ambiguities are integers and when they are not, which is a source of continuing confusion in the literature. Second, it explains how and how not to design GPS receivers so that their carrier-phase measurements are suitable for use in CDGPS relative position estimation algorithms that work with integer ambiguities. Third, it develops a method of doing offline simulation of GPS carrier-phase measurements that is suitable for studying the feasibility and accuracy of proposed CDGPS relative navigation and attitude determination schemes. Fourth, it uses the simulation to evaluate the efficacy of CDGPS techniques for several space-based applications, including applications at high altitude.

The remainder of this paper is divided into five main sections plus conclusions. Section II develops a detailed mathematical model of GPS carrier-phase measurements. Section III analyzes single- and double-differenced carrier-phase measurements and explores when the resulting ambiguities will be integer numbers of carrier cycles. Section IV explains the implications of the model of Sec. II and the analysis of Sec. III for receiver design if the CDGPS estimation scheme needs to resolve ambiguities as integers. Section V presents techniques for doing offline simulations of GPS carrier-phase signals. Section VI gives results from several example simulation studies that explore the efficacy of CDGPS techniques for LEO and GEO applications. Section VII presents the paper's conclusions.

II. Mathematical Model of GPS Carrier-Phase Measurements

This section develops a model of GPS carrier-phase measurements that includes many significant terms. It also presents a pseudorange measurement model (also known as code phase) for the sake of

Presented as Paper 6053 at the Guidance, Navigation, and Control Conference, San Francisco, CA, 15–18 August 2005; received 29 December 2006; revision received 30 April 2007; accepted for publication 30 April 2007.

*Professor, Sibley School of Mechanical and Aerospace Engineering. Associate Fellow AIAA.

†Graduate Student, Sibley School of Mechanical and Aerospace Engineering.

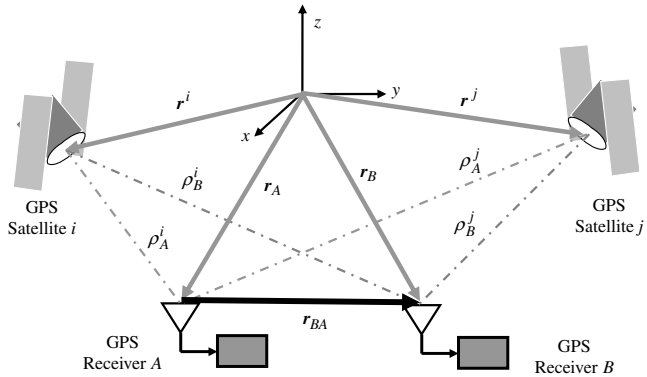

Fig. 1 Geometry of CDGPS measurements for two GPS satellites and two user receivers.

completeness. A code-phase model is useful because some CDGPS techniques also employ code-phase measurements [5,13,14].

The measurement geometry of a typical CDGPS application is depicted in Fig. 1. The user receivers' GPS carrier-phase outputs provide precise measurements of the ranges ρ_A^i, ρ_A^j, ρ_B^i, and ρ_B^j between GPS satellites i and j and receiver antennas A and B. Each of these measurements contains a bias that is termed an ambiguity. CDGPS techniques can estimate the biases and the relative position vector $\boldsymbol{r}_{BA}$ to a high degree of accuracy. These techniques use the range measurements, the known GPS satellite absolute positions $\boldsymbol{r}^i$ and $\boldsymbol{r}^j$, and moderately accurate GPS-based estimates of the absolute user antenna positions $\boldsymbol{r}_A$ and $\boldsymbol{r}_B$. They are based on a measurement model such as the one developed in this section.

A. Time Systems

The model of GPS carrier-phase measurements must consider three different systems for keeping track of time. The first is the true time, which is also called "GPS" time, and is denoted by the variable t. A second time system is that of the receiver clock. The relationship between true time t, receiver clock time t_{RA} at GPS receiver A, and receiver A's clock error δt_{RA} is:

$$t = t_{\mathrm{RA}} - \delta t_{\mathrm{RA}} \tag{1}$$

The third time system is that of the GPS satellite clock. If t^{Sj} is the clock time for GPS satellite j, then the relationship between true time and this satellite's clock time is given by:

$$t^{Sj} = t + a_{f0}^j + a_{f1}^j\left(t - t_{\mathrm{oc}}^j\right) + \delta t_{\mathrm{rel}}^j \tag{2}$$

The parameters a_{f0}^j and a_{f1}^j and the epoch time t_{oc}^j are part of the GPS satellite navigation data message, and $\delta t_{\mathrm{rel}}^j$ is a relativistic correction that depends on the eccentricity, semimajor axis, and eccentric anomaly of the GPS satellite's orbit [15].

These three time systems all affect the measured carrier phase. The erroneous satellite clock is used to generate the original carrier signal. True GPS time is used to measure the propagation delay that affects when a particular part of the carrier signal arrives at the receiver. The erroneous receiver clock is used to generate a carrier replica signal whose phase is differenced with the phase of the received signal to produce the beat phase that is output by the receiver.

B. Position Models and Nominal Transmission Delay

The two fundamental GPS measurements, the pseudorange and the carrier phase, are functions of the transmission delay for the signal to travel from the GPS satellite position to the user antenna position. The nominal transmission time of the signal from satellite j to user antenna A equals the range divided by the speed of light:

$$\delta t_{\mathrm{trn}A}^j = \frac{\rho_A^j}{c} = \frac{\sqrt{[\boldsymbol{r}_A(t) - \boldsymbol{r}^j(t - \delta t_{\mathrm{trn}A}^j)]^T[\boldsymbol{r}_A(t) - \boldsymbol{r}^j(t - \delta t_{\mathrm{trn}A}^j)]}}{c} \tag{3}$$

where c is the speed of light in vacuum. This is an implicit relationship for the transmission delay $\delta t_{\mathrm{trn}A}^j$; it appears on both sides of the equation because it must be used to determine $\boldsymbol{r}^j$ at the transmission time.

C. Line Bias and Ionospheric Effects

All receivers have time delay in the wires from their antennas and in their analog RF components. One of the most significant sources of bias is the delay inherent in the receiver's analog bandpass filters. This bias is modeled as being a constant common-mode, receiver-dependent error, $\delta t_{\ell_n A}$ for receiver A. This bias is normally different for the GPS L1 and L2 frequencies because they use different filters. Thus, it becomes necessary to denote two line biases for a dual-frequency receiver, $\delta t_{\ell_n 1A}$ and $\delta t_{\ell_n 2A}$.

The ionosphere adds a further delay to the GPS code signal that is used to measure pseudorange. The total pseudorange transmission time, including time-of-flight, line bias, and ionospheric effects, is

$$\delta t_{\mathrm{trn}A}^j = \frac{\sqrt{[\boldsymbol{r}_A(t-\delta t_{\ell_n A}) - \boldsymbol{r}^j(t-\delta t_{\mathrm{trn}A}^j)]^T[\boldsymbol{r}_A(t-\delta t_{\ell_n A}) - \boldsymbol{r}^j(t-\delta t_{\mathrm{trn}A}^j)]}}{c} + \delta t_{\mathrm{ion}A}^j + \delta t_{\ell_n A} \tag{4}$$

where

$$\delta t_{\mathrm{ion}A}^j = \frac{40.3\mathrm{TEC}_A^j}{cf^2} \tag{5}$$

The quantity TEC_A^j is the ionospheric total electron content integrated along the line-of-sight (LOS) vector from receiver A to GPS satellite j, and f is the carrier transmission frequency [16].

The ionosphere also causes a carrier-phase advance. This is a positive increment to the received carrier phase in comparison to what it would have been had there been no ionosphere along the signal path. The value of this advance is

$$\delta\phi_{\mathrm{ion}A}^j = f\delta t_{\mathrm{ion}A}^j \tag{6}$$

Tropospheric effects are not modeled in this paper. These effects are not important for space-based user receivers. Appropriate logic can eliminate any signals that pass through a significant portion of the troposphere on their way from the GPS spacecraft to the user receiver.

D. Polarization-Induced Carrier-Phase Windup

The circular polarization of the GPS signal causes a carrier-phase perturbation that is a function of the relative geometries of the transmitting and receiving antennas [11,17]. This geometry is characterized by the unit direction vector that points from GPS satellite j to user receiver A, $\hat{\boldsymbol{\rho}}_A^j$, and by the unit direction vectors that define the transmitter and receiver antenna coordinate systems, $\hat{\boldsymbol{x}}^j$, $\hat{\boldsymbol{y}}^j$, $\hat{\boldsymbol{x}}_A$, and $\hat{\boldsymbol{y}}_A$. Each $(\hat{\boldsymbol{x}}, \hat{\boldsymbol{y}})$ antenna pair is a set of perpendicular vectors whose cross product $\hat{\boldsymbol{x}} \times \hat{\boldsymbol{y}}$ defines the center of the antenna's field of view (FOV). Given these vectors, the perturbation of the received carrier phase is [11]

$$\delta\phi_{\mathrm{pwu}A}^j = \frac{1}{2\pi}\arctan 2\left\{\left[\hat{\boldsymbol{\rho}}_A^j \cdot \left(\hat{\boldsymbol{x}}_{\mathrm{eff}}^j \times \hat{\boldsymbol{x}}_{\mathrm{eff}A}\right)\right], \left(\hat{\boldsymbol{x}}_{\mathrm{eff}}^j \cdot \hat{\boldsymbol{x}}_{\mathrm{eff}A}\right)\right\} \tag{7}$$

where $\arctan 2(,)$ is the usual two-argument arc-tangent function with an output in radians and where the effective x axes of the transmitting and receiving antenna coordinate systems are

$$\hat{\boldsymbol{x}}_{\mathrm{eff}}^j = \hat{\boldsymbol{x}}^j - \hat{\boldsymbol{\rho}}_A^j\left(\hat{\boldsymbol{\rho}}_A^j \cdot \hat{\boldsymbol{x}}^j\right) - \hat{\boldsymbol{\rho}}_A^j \times \hat{\boldsymbol{y}}^j\boldsymbol{s} \tag{8a}$$

$$\hat{\boldsymbol{x}}_{\mathrm{eff}A} = \hat{\boldsymbol{x}}_A - \hat{\boldsymbol{\rho}}_A^j\left(\hat{\boldsymbol{\rho}}_A^j \cdot \hat{\boldsymbol{x}}_A\right) + \hat{\boldsymbol{\rho}}_A^j \times \hat{\boldsymbol{y}}_A \tag{8b}$$

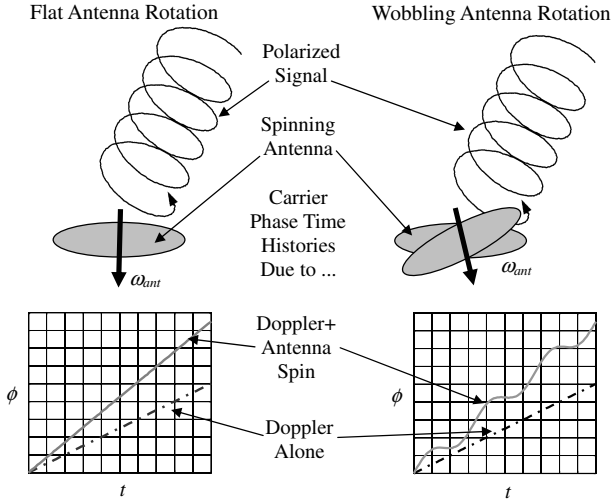

Fig. 2 Differing effects of polarization-induced carrier-phase windup for flat and wobbling antenna rotations.

The significance of this geometric effect is illustrated in Fig. 2. The left-hand side of the figure illustrates what happens when a patch antenna rotates about its FOV centerline while receiving a polarized GPS signal. There is a constant increment to the received Doppler shift that causes the black dash-dotted carrier-phase time history in the lower plot to change into the solid gray curve. The situation on the right-hand side of the figure is one in which the antenna wobbles; it rotates about an axis that is not parallel to the centerline of its FOV. The solid gray carrier-phase time history in the lower right-hand part of the figure has a Doppler shift bias plus a periodic phase variation due to the wobble. The Doppler bias does not impact CDGPS techniques because it acts like a common-mode clock frequency error on all signals. The periodic phase variations can be different for different GPS satellite signals and for different receivers; therefore, they have the potential to negatively impact CDGPS techniques.

E. Multipath, Antenna Phase-Center Variation, and Thermal Noise

Signal reflections off of the user spacecraft give rise to a multipath carrier-phase error that depends on the direction of arrival of the signal $\hat{\boldsymbol{\rho}}_A^j$ and on the attitude of the user spacecraft. This error is denoted as $\delta\phi_{\text{mp}A}^j$. Typical rms levels of carrier-phase multipath error are $\sigma_{\text{mp}A}^j = (0.005\text{ m})/\lambda$ cycles [18], where λ is the wavelength. Note, however, that complex spacecraft with large reflective surfaces, such as the International Space Station, might have larger multipath errors. The multipath errors for the L1 and L2 frequencies of dual-frequency systems are the independent quantities $\delta\phi_{\text{mp1}A}^j$ and $\delta\phi_{\text{mp2}A}^j$.

Antenna phase-center variations also produce a carrier-phase error that is a function of the arrival signal direction and the user spacecraft attitude. This error source may yield a carrier-phase perturbation as large as $(0.01\text{ m})/\lambda$ cycles [11]. This error is lumped into $\delta\phi_{\text{mp}A}^j$ for modeling purposes because it has the same geometric dependence as the multipath error if the multipath signals do not come from articulating or highly deformable reflective surfaces.

Carrier-phase thermal noise errors $n_{\phi A}^j$ are the result of random electrical noise received by the antenna and generated in the receiver's RF front end. This error source can be modeled as Gaussian white noise if the sampling frequency is no greater than the bandwidth of the receiver's phase-lock loop (PLL). Its standard deviation is determined from the received carrier-to-noise ratio C/N_0 and the PLL bandwidth B_{PLL}:

$$\sigma_{n\phi A}^j = \frac{1}{2\pi}\sqrt{\frac{B_{\text{PLL}}}{2C/N_0}}\text{ cycles} \tag{9}$$

Dual-frequency receivers have independent thermal noise errors for each frequency, $n_{\phi 1A}^j$ and $n_{\phi 2A}^j$. The thermal noise error model in Eq. (9) applies to signals on the L2 frequency only if working with a military receiver or a civilian receiver that can track the new L2C signals.

F. Complete Carrier-Phase Measurement Model

The measured carrier phase is the difference between a receiver-generated replica of the nominal carrier phase and the received carrier phase as determined by the receiver's PLL. An analysis of the L1 carrier-phase measurement starts with the phase time history of the transmitted signal:

$$\begin{aligned}\psi_{10}^j + f_{L1}t^{Sj} &= \psi_{10}^j + f_{L1}\left[t + a_{f0}^j + a_{f1}^j\left(t - t_{\text{oc}}^j\right) + \delta t_{\text{rel}}^j\right] \\ &= \left[\psi_{10}^j + f_{L1}\left(a_{f0}^j - a_{f1}^j t_{\text{oc}}^j + \delta t_{\text{rel}}^j\right)\right] + f_{L1}\left(1 + a_{f1}^j\right)t\end{aligned} \tag{10}$$

where ψ_{10}^j is the initial transmitted L1 carrier phase when the erroneous satellite clock time is $t^{Sj} = 0$ and where $f_{L1} = 1575.42$ MHz is the nominal L1 broadcast frequency.

The received carrier phase equals the transmitted carrier phase with corrections for transmission delay, ionospheric delay, polarization phase windup, multipath, phase-center variation, and thermal noise:

$$\begin{aligned}\psi_{1A}^j(t) = &\left[\psi_{10}^j + f_{L1}\left(a_{f0}^j - a_{f1}^j t_{\text{oc}}^j + \delta t_{\text{rel}}^j\right)\right] + f_{L1}\left(1 + a_{f1}^j\right)\left[t - \delta t_{\text{trn}A}^j\right] \\ &+ 2f_{L1}\left(1 + a_{f1}^j\right)\delta t_{\text{ion}A}^j + \delta\phi_{\text{pwu}A}^j + \delta\phi_{\text{mp1}A}^j + n_{\phi 1A}^j\end{aligned} \tag{11}$$

The extra factor of two in the ionospheric term counteracts the effect of the ionospheric delay in the $\delta t_{\text{trn}A}^j$ formula of Eq. (4).

The receiver's replica of the nominal L1 carrier signal phase takes the form

$$\gamma_{1A}^j(t_{\text{RA}}) = \gamma_{10A}^j + f_{L1}t_{\text{RA}} \tag{12}$$

where γ_{10A}^j is the initial replica L1 carrier phase when the erroneous receiver clock time is $t_{\text{RA}} = 0$. This initial phase varies with the received satellite j because of full-cycle ambiguities in how the PLL locks onto signals. There may be additional variations of this quantity from satellite to satellite if the receiver is not designed properly. Section IV discusses this issue.

The GPS carrier-phase observable is the difference between the replica nominal phase in Eq. (12) and the received phase in Eq. (11). This difference yields

$$\begin{aligned}\phi_{1A}^j(t_{\text{RA}}) = &\gamma_{1A}^j(t_{\text{RA}}) - \psi_{1A}^j(t_{\text{RA}} - \delta t_{\text{RA}}) \\ = &\gamma_{10A}^j + f_{L1}t_{\text{RA}} - \left[\psi_{10}^j + f_{L1}\left(a_{f0}^j - a_{f1}^j t_{\text{oc}}^j + \delta t_{\text{rel}}^j\right)\right] \\ &- f_{L1}\left(1 + a_{f1}^j\right)\left[t_{\text{RA}} - \delta t_{\text{RA}} - \delta t_{\text{trn}A}^j\right] \\ &- 2f_{L1}\left(1 + a_{f1}^j\right)\delta t_{\text{ion}A}^j - \delta\phi_{\text{pwu}A}^j - \delta\phi_{\text{mp1}A}^j - n_{\phi 1A}^j = \frac{\left(1 + a_{f1}^j\right)}{\lambda_{L1}} \\ &\times\sqrt{\left[\Delta\boldsymbol{r}_A^j\left(t_{\text{RA}} - \delta t_{\text{RA}}, \delta t_{\ell_{\text{n}}1A}, \delta t_{\text{trn}A}^j\right)\right]^T\Delta\boldsymbol{r}_A^j\left(t_{\text{RA}} - \delta t_{\text{RA}}, \delta t_{\ell_{\text{n}}1A}, \delta t_{\text{trn}A}^j\right)} \\ &+ f_{L1}\left(1 + a_{f1}^j\right)\delta t_{\text{RA}} + \left[\gamma_{10A}^j - \psi_{10}^j - f_{L1}\left(a_{f0}^j - a_{f1}^j t_{\text{oc}}^j + \delta t_{\text{rel}}^j\right)\right] \\ &- f_{L1}a_{f1}^j t_{\text{RA}} - \frac{40.3\text{TEC}_A^j}{cf_{L1}\left(1 + a_{f1}^j\right)} - \delta\phi_{\text{pwu}A}^j + f_{L1}\left(1 + a_{f1}^j\right)\delta t_{\ell_{\text{n}}1A} \\ &- \delta\phi_{\text{mp1}A}^j - n_{\phi 1A}^j\end{aligned} \tag{13}$$

where Eqs. (1), (4), and (5) have been used to eliminate t and $\delta t_{\text{ion}A}^j$ and to partially eliminate $\delta t_{\text{trn}A}^j$ and where $\Delta\boldsymbol{r}_A^j(t, \delta t_{\ell_{\text{n}}1A}, \delta t_{\text{trn}A}^j) = [\boldsymbol{r}_A(t - \delta t_{\ell_{\text{n}}1A}) - \boldsymbol{r}^j(t - \delta t_{\text{trn}A}^j)]\boldsymbol{L}$. Multiplication of both sides of Eq. (13) by the nominal L1 carrier wavelength λ_{L1} and rearrangement of terms yields the standard equation

$$\lambda_{L1}\phi^j_{1A}(t_{\mathrm{RA}}) = \left(1+a^j_{f1}\right) \times \sqrt{\left[\Delta \boldsymbol{r}^j_A\left(t_{\mathrm{RA}}-\delta t_{\mathrm{RA}},\delta t_{\ell_{\mathrm{n}}1A},\delta t^j_{\mathrm{trn}A}\right)\right]^T \Delta \boldsymbol{r}^j_A\left(t_{\mathrm{RA}}-\delta t_{\mathrm{RA}},\delta t_{\ell_{\mathrm{n}}1A},\delta t^j_{\mathrm{trn}A}\right)} + c\left(1+a^j_{f1}\right)\left(\delta t_{\mathrm{RA}}+\delta t_{\ell_{\mathrm{n}}1A}\right) - c\left[a^j_{f0}+a^j_{f1}\left(t_{\mathrm{RA}}-t^j_{\mathrm{oc}}\right)+\delta t^j_{\mathrm{rel}}\right] + \lambda_{L1}\left(\gamma^j_{10A}-\psi^j_{10}\right) - \frac{40.3\,\mathrm{TEC}^j_A}{f^2_{L1}\left(1+a^j_{f1}\right)} - \lambda_{L1}\left[\delta\phi^j_{\mathrm{pwu}A}+\delta\phi^j_{\mathrm{mp1}A}+n^j_{\phi 1A}\right] \tag{14}$$

It is instructive to compare Eq. (14) to other carrier-phase measurement formulations in the literature, such as Eq. 13 of [3], Eq. (5.32) of [10], or Eq. (5.10) of [11]. The first three terms on the right-hand side are the usual range, receiver-clock-error, and transmitter-clock-error terms. They include corrections for receiver line bias, the effect of satellite clock frequency error on the transmitted carrier wavelength, and relativity. The satellite clock frequency errors a^j_{f1} typically have magnitudes less than 5×10^{-11}. When multiplied by maximal differential ranges of ±7000 km, the resulting errors are 0.35 mm or less, which are negligible. Retention of the a^j_{f1} terms makes the model applicable for future signals that might have larger a^j_{f1} values.

The most interesting term in Eq. (14) is the fourth term on the right-hand side, which equals the carrier-phase increment $(\gamma^j_{10A}-\psi^j_{10})$ times λ_{L1}. The literature calls this increment the carrier-phase ambiguity. It is often called the integer ambiguity, as in [3,11], but this is a misnomer because it is not restricted to integer values. Its first component is the phase of the receiver's nominal carrier replica at receiver time $t_{\mathrm{RA}}=0$, and its second component is the carrier phase at the transmitter antenna at GPS satellite time $t^{Sj}=0$. There is no reason for either of these initial phases to be integers or for their difference to be an integer. Although [10] offers little or no insight about the genesis of its equivalent terms, it comes close to the ambiguity model of Eq. (14) by breaking its ambiguity into a real-valued term that depends on initial phases plus an integer ambiguity. Its model does not recognize that the real-valued initial phase of the receiver replica can vary for different GPS satellites if the receiver has not been configured with CDGPS applications in mind. Thus, its formulation cannot be used to guide proper receiver design. Section III discusses the issue of carrier-phase ambiguities and when they can be expected to take on integer values.

There is an equivalent carrier-phase measurement equation for the L2 signal. The only differences between it and Eq. (14) are that the 1s in the subscripts of the quantities λ_{L1}, f_{L1}, ϕ^j_{1A}, γ^j_{10A}, ψ^j_{10}, $\delta\phi^j_{\mathrm{mp1}A}$, $n^j_{\phi 1A}$, and $\delta t_{\ell_{\mathrm{n}}1A}$ get replaced by 2s.

G. Pseudorange Measurement Model

The pseudorange measurement equations are included here for the sake of completeness. The L1 pseudorange equation takes the form

$$P^j_{1A}(t_{\mathrm{RA}}) = \sqrt{\left[\Delta \boldsymbol{r}^j_A\left(t_{\mathrm{RA}}-\delta t_{\mathrm{RA}},\delta t_{\ell_{\mathrm{n}}1A},\delta t^j_{\mathrm{trn}A}\right)\right]^T \Delta \boldsymbol{r}^j_A\left(t_{\mathrm{RA}}-\delta t_{\mathrm{RA}},\delta t_{\ell_{\mathrm{n}}1A},\delta t^j_{\mathrm{trn}A}\right)} + c(\delta t_{\mathrm{RA}}+\delta t_{\ell_{\mathrm{n}}1A}) - c\left[a^j_{f0}+a^j_{f1}\left(t_{\mathrm{RA}}-\delta t_{\mathrm{RA}}-\delta t^j_{\mathrm{trn}A}-t^j_{\mathrm{oc}}\right)+\delta t^j_{\mathrm{rel}}\right] + \frac{40.3\,\mathrm{TEC}^j_A}{f^2_{L1}\left(1+a^j_{f1}\right)^2} + n^j_{P1A} \tag{15}$$

This equation is similar to the carrier-phase model in Eq. (14), but it does not have a carrier-phase ambiguity, and it lumps most of the transmitter-clock-error effects into the third term on its right-hand side. Multipath error is not included in Eq. (15) because code multipath error is not expected to be large for satellites that do not have large reflecting surfaces in the FOV of the GPS antenna, nor does code multipath error have a large impact on the accuracy of the CDGPS algorithms that might be developed using this paper's models. The standard deviation of the code range thermal noise error n^j_{P1A} is a function of the received carrier-to-noise ratio, the delay-lock loop (DLL) bandwidth, B_{DLL}, the spacing between the early and late code accumulations used in the DLL's noncoherent dot-product discriminator t_{eml}, the chip period of the pseudorandom number code that gets used to measure pseudorange t_c, and the predetection integration time of the accumulations used in the DLL's discriminator t_{acc} [19]:

$$\sigma^j_{nPA} = ct_c\sqrt{\frac{B_{\mathrm{DLL}}t_{\mathrm{eml}}}{2t_cC/N_0}\left(1+\frac{1}{t_{\mathrm{acc}}C/N_0}\right)} \tag{16}$$

This error can be modeled as Gaussian white noise if the pseudorange sampling rate is lower than the DLL bandwidth.

An equation similar to Eq. (15) applies for the L2 pseudorange. The only differences are changes from subscripts of 1 to subscripts of 2 in the terms P^j_{1A}, f_{L1}, $\delta t_{\ell_{\mathrm{n}}1A}$, and n^j_{P1A} to distinguish them from the corresponding L1 terms. The applicability of the Eq. (16) thermal noise error model to L2 signals presumes the use of either a military receiver or a civilian receiver that tracks the new L2C signals.

III. Single- and Double-Differenced Carrier-Phase Measurements and Ambiguities

Differencing of GPS carrier-phase measurements is used to eliminate common-mode errors. Differencing also may yield true integer ambiguities. The goal of this section is to understand the situations in which differencing produces integer ambiguities.

A. Single-Differenced Carrier Phase

The most common single-differenced carrier-phase measurement is the difference between the signal that is produced by the same GPS satellite and received by two different user antennas. It removes common-mode errors generated at the GPS satellite. Suppose that the signal from satellite j is tracked by receivers A and B. Then the single-differenced L1 carrier-phase measurement model is

$$\lambda_{L1}[\phi^j_{1A}(t_{\mathrm{RA}})-\phi^j_{1B}(t_{\mathrm{RB}})] = (1+a^j_{f1}) \times \sqrt{[\Delta \boldsymbol{r}^j_A(t_{\mathrm{RA}}-\delta t_{\mathrm{RA}},\delta t_{\ell_{\mathrm{n}}1A},\delta t^j_{\mathrm{trn}A})]^T \Delta \boldsymbol{r}^j_A(t_{\mathrm{RA}}-\delta t_{\mathrm{RA}},\delta t_{\ell_{\mathrm{n}}1A},\delta t^j_{\mathrm{trn}A})} - (1+a^j_{f1}) \times \sqrt{[\Delta \boldsymbol{r}^j_B(t_{\mathrm{RB}}-\delta t_{\mathrm{RB}},\delta t_{\ell_{\mathrm{n}}1B},\delta t^j_{\mathrm{trn}B})]^T \Delta \boldsymbol{r}^j_B(t_{\mathrm{RB}}-\delta t_{\mathrm{RB}},\delta t_{\ell_{\mathrm{n}}1B},\delta t^j_{\mathrm{trn}B})} + c\left(1+a^j_{f1}\right)[\delta t_{\mathrm{RA}}+\delta t_{\ell_{\mathrm{n}}1A}-\delta t_{\mathrm{RB}}-\delta t_{\ell_{\mathrm{n}}1B}] - ca^j_{f1}[t_{\mathrm{RA}}-t_{\mathrm{RB}}]+\lambda_{L1}\left[\gamma^j_{10A}-\gamma^j_{10B}\right]-\frac{40.3\,\mathrm{TEC}^j_A}{f^2_{L1}(1+a^j_{f1})} + \frac{40.3\,\mathrm{TEC}^j_B}{f^2_{L1}\left(1+a^j_{f1}\right)} - \lambda_{L1}\left[\delta\phi^j_{\mathrm{pwu}A}-\delta\phi^j_{\mathrm{pwu}B}+\delta\phi^j_{\mathrm{mp1}A} - \delta\phi^j_{\mathrm{mp1}B}+n^j_{\phi 1A}-n^j_{\phi 1B}\right] \tag{17}$$

Equation (17) can be simplified by using the single-differenced operator notation $\Delta()^j_{AB} = ()^j_A - ()^j_B$, that is, the placement of a Δ in front of a quantity and the use of the subscript $()_{AB}$ after it indicates a difference of that quantity between receivers A and B. If one also uses the following shorthand for the range

$$\rho^j_A = \sqrt{\left[\Delta \boldsymbol{r}^j_A\left(t_{\mathrm{RA}}-\delta t_{\mathrm{RA}},\delta t_{\ell_{\mathrm{n}}1A},\delta t^j_{\mathrm{trn}A}\right)\right]^T \Delta \boldsymbol{r}^j_A\left(t_{\mathrm{RA}}-\delta t_{\mathrm{RA}},\delta t_{\ell_{\mathrm{n}}1A},\delta t^j_{\mathrm{trn}A}\right)} \tag{18}$$

then Eq. (17) simplifies to

$$\lambda_{L1}\Delta\phi^j_{1AB} = \left(1+a^j_{f1}\right)\Delta\rho^j_{AB} + c\left(1+a^j_{f1}\right)(\Delta\delta t_{\rm RAB} + \Delta\delta t_{\ell_n\,1AB}) - ca^j_{f1}\Delta t_{\rm RAB} + \lambda_{L1}\Delta\gamma^j_{10AB} - \frac{40.3\Delta{\rm TEC}^j_{AB}}{f^2_{L1}\left(1+a^j_{f1}\right)} - \lambda_{L1}\left[\Delta\delta\phi^j_{{\rm pwu}AB} + \Delta\delta\phi^j_{{\rm mp1}AB} + \Delta n^j_{\phi 1AB}\right] \quad (19)$$

This equation does not include the usual satellite ephemeris error term. The formulation in Eq. (19) presumes that $\boldsymbol{r}^j(t)$ is the true satellite position time history, not that reported by the navigation message. The distinction between these two time histories is addressed in the discussion of simulation in Sec. V.

A comparison between Eqs. (19) and (14) illustrates the advantage of taking this single difference: all of the terms that depend only on the satellite, i.e., only on j, have been eliminated. These include the initial transmitted carrier phase, the initial satellite clock error, and the relativistic term. The cancellation of this latter term is based on the reasonable assumption that it varies slowly with time.

The single-differenced carrier-phase ambiguity in Eq. (19) is $\Delta\gamma^j_{10AB} = \gamma^j_{10A} - \gamma^j_{10B}$, which appears in the fourth term on the right-hand side. The initial phases of the receivers' carrier replicas, γ^j_{10A} and γ^j_{10B}, are determined by the receiver's RF front-end down-conversion operations and its software. There is no reason to expect the difference of these two initial phases to be an integer if receivers A and B operate independently. Thus, it is normally not possible to resolve a single-differenced carrier-phase ambiguity as an integer.

If the two receivers are linked, however, then $\Delta\gamma^j_{10AB}$ will be an integer if the receivers are properly designed. The usual application in which proper linking occurs is GPS attitude determination. In this case, the two receivers have RF front-ends whose mixing chains and sampling clocks are phase-locked to a common oscillator. These features, when coupled with the proper baseband signal processing software, can be used to guarantee that the single-differenced carrier-phase ambiguity $\Delta\gamma^j_{10AB}$ is an integer.

The following are additional advantages of an attitude determination system: closeness of the antennas implies that the single-differenced ionospheric correction is zero, $\Delta{\rm TEC}^j_{AB} = 0$. The known relative antenna orientations imply that the polarization term $\Delta\delta\phi^j_{{\rm pwu}AB}$ can either be eliminated by antenna alignment or by a calibration [17]. The differential line bias $\Delta\delta t_{\ell_n\,1AB}$ can be calibrated out. The time difference $\Delta t_{\rm RAB}$ is zero because the receivers use the same clock. The remaining noise terms are the single-differenced multipath and thermal noise, $\Delta\delta\phi^j_{{\rm mp1}AB}$ and $\Delta n^j_{\phi 1AB}$. These are usually small enough to allow a CDGPS attitude estimation algorithm to resolve $\Delta\gamma^j_{10AB}$ as an integer.

B. Double-Differenced Carrier Phase

Double-differencing between two GPS satellites can be used to remove receiver-generated common-mode errors from the single differences between two receivers. If one defines the double-differenced operator $\nabla\Delta(\,)^{ij}_{AB} = \Delta(\,)^i_{AB} - \Delta(\,)^j_{AB} = (\,)^i_A - (\,)^i_B - (\,)^j_A + (\,)^j_B$, then the double-differenced L1 carrier-phase measurement for satellites i and j and receivers A and B is

$$\lambda_{L1}\nabla\Delta\phi^{ij}_{1AB} = \nabla\Delta\rho^{ij}_{AB} + \lambda_{L1}\nabla\Delta\gamma^{ij}_{10AB} - \frac{40.3\nabla\Delta{\rm TEC}^{ij}_{AB}}{f^2_{L1}} - \lambda_{L1}\left[\nabla\Delta\delta\phi^{ij}_{{\rm pwu}AB} + \nabla\Delta\delta\phi^{ij}_{{\rm mp1}AB} + \nabla\Delta n^{ij}_{\phi 1AB}\right] + c\left(a^i_{f1} - a^j_{f1}\right)[\Delta\delta t_{\rm RAB} + \Delta\delta t_{\ell_n\,1AB} - \Delta t_{\rm RAB}] \quad (20)$$

This formulation assumes the following nonstandard definitions of the range and TEC double-differences:

$$\nabla\Delta\rho^{ij}_{AB} = \left(1+a^i_{f1}\right)\Delta\rho^i_{AB} - \left(1+a^j_{f1}\right)\Delta\rho^j_{AB} \quad (21a)$$

$$\nabla\Delta{\rm TEC}^{ij}_{AB} = \frac{\Delta{\rm TEC}^i_{AB}}{\left(1+a^i_{f1}\right)} - \frac{\Delta{\rm TEC}^j_{AB}}{\left(1+a^j_{f1}\right)} \quad (21b)$$

These definitions account for the different satellite clock frequency errors a^i_{f1} and a^j_{f1}.

The term on the right-hand side of Eq. (20) that has the coefficient $(a^i_{f1} - a^j_{f1})$ is a residual satellite clock correction term. It does not normally appear in double-differenced measurement models. Its $\Delta\delta t_{\rm RAB}$ and $\Delta\delta t_{\ell_n\,1AB}$ components are normally negligible, but its $\Delta t_{\rm RAB}$ component can be significant. The value of $\Delta t_{\rm RAB}$ is known, which implies that this term can be subtracted out of the measurement equation. This subtraction allows double-differences to be used even for receivers whose sample times are not synchronized.

The double-differenced carrier-phase ambiguity in Eq. (20) is $\nabla\Delta\gamma^{ij}_{10AB} = \gamma^i_{10A} - \gamma^i_{10B} - \gamma^j_{10A} + \gamma^j_{10B}$. If receivers A and B are designed properly, then the quantities $(\gamma^i_{10A} - \gamma^j_{10A})$ and $(\gamma^i_{10B} - \gamma^j_{10B})$ will both be integers, and the ambiguity $\nabla\Delta\gamma^{ij}_{10AB}$ will be an integer because it is the difference of two integers. Section IV discusses the receiver design requirements which guarantee that $(\gamma^i_{10A} - \gamma^j_{10A})$ and $(\gamma^i_{10B} - \gamma^j_{10B})$ will be integers.

The double-differenced ionospheric error $\nabla\Delta{\rm TEC}^{ij}_{AB}$ should be negligible if the baseline between receivers A and B is short. If the baseline is long, then dual-frequency measurements and processing may be needed to correct for a non-negligible $\nabla\Delta{\rm TEC}^{ij}_{AB}$ value.

The circular polarization windup term $\nabla\Delta\delta\phi^{ij}_{{\rm pwu}AB}$ may be significant. In terrestrial applications, this term is often negligible because of the short baselines involved and because the receiving antennas all point upwards. In spacecraft applications, this term may grow to be significant for long baselines or if the spacecraft attitudes are significantly different. If this happens, then attitude knowledge must be used to compensate for this term; otherwise, it will not be possible to estimate integer ambiguities. To the best knowledge of the authors, no other work on relative spacecraft navigation has considered the effects of this term. Given that all studies of space-based CDGPS have been simulation studies and given that current simulators do not include this effect, this term could cause an unpleasant surprise during an actual flight experiment. This issue is revisited in the simulation results of Sec. VI.

If the errors from the ionosphere and the circular polarization are sufficiently small, then double-differenced carrier-phase ambiguities should be resolvable as integers. The other errors are the double-differenced multipath, $\nabla\Delta\delta\phi^{ij}_{{\rm mp1}AB}$, and the double-differenced thermal noise, $\nabla\Delta n^{ij}_{\phi 1AB}$. These errors are normally small enough to allow integer ambiguity resolution.

C. Error Covariance Models

It is necessary to compute correct error covariance matrices if one wants to process single- and double-differenced carrier-phase measurements optimally. The variances of the single-differenced errors $\Delta\delta\phi^j_{{\rm mp1}AB}$ and $\Delta n^j_{\phi 1AB}$ can be computed from the variances of the original errors $\delta\phi^j_{{\rm mp1}A}$, $\delta\phi^j_{{\rm mp1}B}$, $n^j_{\phi 1A}$, and $n^j_{\phi 1B}$:

$$(\sigma^j_{\Delta\phi{\rm mp1}AB})^2 = (\sigma^j_{\phi{\rm mp1}A})^2 + (\sigma^j_{\phi{\rm mp1}B})^2 \quad (22a)$$

$$(\sigma^j_{\Delta n\phi 1AB})^2 = (\sigma^j_{n\phi 1A})^2 + (\sigma^j_{n\phi 1B})^2 \quad (22b)$$

There is no cross correlation between the single-differenced errors for different GPS signals. In other words, $E\{\Delta\delta\phi^i_{{\rm mp1}AB}\Delta\delta\phi^j_{{\rm mp1}AB}\} = E\{\Delta n^i_{\phi 1AB}\Delta n^j_{\phi 1AB}\} = 0$ for all $i \neq j$.

Double-differenced errors have variances and cross correlations. The variances of double-differenced errors are computed from the single-differenced error variances:

$$\left(\sigma^{ij}_{\nabla\Delta\phi{\rm mp1}AB}\right)^2 = \left(\sigma^i_{\Delta\phi{\rm mp1}AB}\right)^2 + \left(\sigma^j_{\Delta\phi{\rm mp1}AB}\right)^2 \quad (23a)$$

$$\left(\sigma^{ij}_{\nabla\Delta n\phi 1AB}\right)^2 = \left(\sigma^i_{\Delta n\phi 1AB}\right)^2 + \left(\sigma^j_{\Delta n\phi 1AB}\right)^2 \quad (23b)$$

Cross correlation of double-differenced measurements arises because the differences are normally computed between a nominal GPS satellite signal, call this signal j, and all the other signals. Given two other signals i and k, the cross correlations of their computed double-differences with satellite j are

$$E\left\{\nabla\Delta\delta\phi^{ij}_{\text{mp1}AB}\nabla\Delta\delta\phi^{kj}_{\text{mp1}AB}\right\} = (\sigma^j_{\Delta\phi\text{mp1}AB})^2 \tag{24a}$$

$$E\left\{\nabla\Delta n^{ij}_{\phi 1AB}\nabla\Delta n^{kj}_{\phi 1AB}\right\} = (\sigma^j_{\Delta n\phi 1AB})^2 \tag{24b}$$

IV. Receiver Design Requirements for Differential Carrier-Phase Measurements

A. Three Requirements

There are three design requirements that must be met in order for a GPS receiver's carrier-phase measurements to be useful for general CDGPS calculations. These requirements will be discussed in terms of the L1 signal with the understanding that similar requirements hold for L2 in a dual-frequency receiver. Subsection IV.C discusses an additional requirement that is specific to dual-frequency receivers. The first two requirements concern the measurement of the received carrier phase $\psi^j_{1A}(t_{\text{RA}} - \delta t_{\text{RA}})$. The third requirement concerns generation of the receiver's nominal carrier phase $\gamma^j_{1A}(t_{\text{RA}})$.

The first requirement is that the receiver use a PLL to track the received carrier signal. A PLL enables the receiver to make precise measurements of $\psi^j_{1A}(t_{\text{RA}} - \delta t_{\text{RA}})$ with bounded errors that do not drift significantly with time. Drift errors cannot be tolerated in CDGPS calculations because they translate into drift of the ambiguities and destroy the ability to resolve the ambiguities as constants. The receiver should use a third-order PLL so that the measured carrier phase does not have any biases as a result of range accelerations between the GPS spacecraft and the user receiver [19].

The second requirement is that the receiver resolve a 180 deg phase ambiguity in its measured value of $\psi^j_{1A}(t_{\text{RA}} - \delta t_{\text{RA}})$. This ambiguity is the result of the transmission of navigation data bits on the signal using binary phase shift keying (BPSK). By itself, the receiver's PLL cannot tell the difference between positive and negative data bits. The receiver must decode the navigation data bits and use known bit patterns within the data to distinguish positive data bits from negative data bits. Once the data bits have been decoded, it is straightforward to determine and apply the necessary adjustment to the measured phase $\psi^j_{1A}(t_{\text{RA}} - \delta t_{\text{RA}})$. This adjustment is 0 cycles if the raw data bits have the correct signs, and it is $+0.5$ cycles if they have incorrect signs. If this requirement is not met, then the carrier-phase ambiguities discussed in this paper can be multiples of one-half, i.e., ambiguities such as $\nabla\Delta\gamma^{ij}_{10AB} = 11.5$ are possible.

The third requirement is that the receiver generate its nominal carrier-phase signal for each tracked GPS signal in a way that causes any two nominal initial phases for any two satellites i and j to differ by an exact integer number of cycles. That is

$$\gamma^i_{10A} - \gamma^j_{10A} = N^{ij}_A \tag{25}$$

for some integer N^{ij}_A.

A receiver must have two properties to meet this requirement. First, the RF front-end's analog frequency down-conversion process must be performed identically for all GPS signals. Typical designs meet this requirement by using a single superheterodyne mixing RF front-end. The frequency down-conversion process effectively generates the satellite j mixing signal phase $\alpha^j(t_{\text{RA}}) = \alpha^j_0 + f_{\text{mix}}t_{\text{RA}}$ with initial value α^j_0 and mixing frequency f_{mix}. This phase is a component of the satellite j nominal carrier-phase signal: $\gamma^j_{1A}(t_{\text{RA}}) = \alpha^j(t_{\text{RA}}) + \eta^j(t_{\text{RA}})$. The other component, $\eta^j(t_{\text{RA}}) = \eta^j_0 + f_{\text{if}}t_{\text{RA}}$, is the phase of the nominal intermediate-frequency carrier signal at the output of the RF front-end. Its initial value is η^j_0 and its intermediate frequency is $f_{\text{if}} = f_{L1} - f_{\text{mix}}$. Although the values of the initial mixing phases α^i_0 and α^j_0 are typically unknown, their difference is guaranteed to be an exact integer number of cycles. Therefore, the mixing components' contribution to the difference in Eq. (25) is an integer.

The remaining property needed by the receiver is that $\eta^i_0 - \eta^j_0$ be an integer for every pair of satellites i and j. Modern receivers typically use digital computations to generate the signals $\eta^i(t_{\text{RA}})$ and $\eta^j(t_{\text{RA}})$ and to difference them with the corresponding received phases that are output by the PLLs that track satellites i and j. One obvious way to ensure that $\eta^i_0 - \eta^j_0$ is an integer is to use $\eta^i_0 = \eta^j_0$ for all satellite pairs, i.e., to use a single nominal intermediate-frequency carrier-phase signal for all tracked GPS satellites. Unfortunately, some receivers' frequency plans make this approach impractical. If the intermediate carrier frequency f_{if} is large, then $\eta^j(t_{\text{RA}})$ will overflow a digital storage word in a short amount of time. Therefore, a receiver with a large f_{if} value does not generate and store $\eta^j(t_{\text{RA}})$ as an independent quantity. Fortunately, alternate strategies exist for ensuring that $\eta^i_0 - \eta^j_0$ is an integer in this situation. One such strategy is described in the following example.

B. Carrier-Phase Processing in an Example Receiver

This section describes good and bad carrier-phase measurement processing in a typical L1 receiver. The example receiver's RF front-end performs high-side mixing of the incoming signal with a signal whose phase time history is

$$\alpha(t_{\text{RA}}) = \alpha_0 + (f_{L1} + f_{\text{if}})t_{\text{RA}} \tag{26}$$

The target intermediate frequency of the L1 signal after mixing is f_{if}, and α_0 is the initial phase of the mixing signal. The notation in Eq. (26) conflicts with the notation of the previous subsection due to the use of high-side mixing. The mixing signal frequency of the previous subsection is $f_{L1} - f_{\text{if}}$, but it is $f_{L1} + f_{\text{if}}$ in this example. This source of confusion is tolerated because it simplifies the discussion of the example and because the example deals with a common receiver design. Note that $\alpha(t_{\text{RA}})$ does not require a superscript to identify the associated GPS satellite because this mixing signal is the same for all satellites.

The signal phase of satellite j at the output of the RF front-end is

$$\beta^j(t_{\text{RA}}) = \alpha(t_{\text{RA}}) - \psi^j_{1A}(t_{\text{RA}}) \tag{27}$$

The receiver's PLL tracks this signal and returns the following incremental $\beta^j(t_{\text{RA}})$ data at each sample time $t_{\text{RA}k}$:

$$\Delta\beta^j_k = \text{floor}[\beta^j(t_{\text{RA}k})] - \text{floor}[\beta^j(t_{\text{RA}(k-1)})] \tag{28a}$$

$$\delta\beta^j_k = \beta^j(t_{\text{RA}k}) - \text{floor}[\beta^j(t_{\text{RA}k})] \tag{28b}$$

where the floor[ ] function rounds its input argument to the nearest integer in the direction of $-\infty$. $\Delta\beta^j_k$ is the number of full cycles of the tracked intermediate-frequency signal that are completed during the sample interval from time $t_{\text{RA}(k-1)}$ to time $t_{\text{RA}k}$, and $\delta\beta^j_k$ is the current fractional part of the intermediate signal's phase. The PLL hardware outputs $\beta^j(t_{\text{RA}})$ data in this incremental form because absolute $\beta^j(t_{\text{RA}})$ data would require the storage of very large numbers due to the high value of f_{if}; a typical nominal intermediate frequency is $f_{\text{if}} = 1.405397$ MHz.

The following candidate algorithm recursively computes $\phi^j_{1A}(t_{\text{RA}k})$ based on the data defined in Eqs. (28a) and (28b).

1) Initiate tracking of satellite j at receiver clock time $t_{\text{RA}k_j}$ and set $\phi^j_{1A}(t_{\text{RA}k_j}) = 0$.

2) At each sample time $t_{\text{RA}k} > t_{\text{RA}k_j}$ compute $\phi^j_{1A}(t_{\text{RA}k})$ based on data from the preceding sample time and based on the PLL outputs according to the formula

$$\phi^j_{1A}(t_{\text{RA}k}) = \phi^j_{1A}(t_{\text{RA}(k-1)}) + \left[\Delta\beta^j_k + \delta\beta^j_k - \delta\beta^j_{k-1}\right] - f_{\text{if}}[t_{\text{RA}k} - t_{\text{RA}(k-1)}] \tag{29}$$

The second term on the right-hand side of Eq. (29) is the increment to $\beta^j(t_{\mathrm{RA}})$ during the interval from $t_{\mathrm{RA}(k-1)}$ to $t_{\mathrm{RA}k}$, and the last term is the nominal increment that $\beta^j(t_{\mathrm{RA}})$ would undergo if there were no Doppler shift.

This initialization and update scheme for the beat carrier phase is consistent with the measurement model in Eq. (14). It is not the best scheme to use, however, because it fails to guarantee that double-differenced carrier-phase ambiguities will be integers. If this carrier-phase processing scheme is used, then the difference of the initial phases of the nominal beat signals of satellites i and j is

$$\gamma^i_{10A} - \gamma^j_{10A} = \psi^i_{1A}(t_{\mathrm{RA}k_i}) - \psi^j_{1A}(t_{\mathrm{RA}k_j}) + f_{L1}[t_{\mathrm{RA}k_j} - t_{\mathrm{RA}k_i}] \quad (30)$$

There is no reason for this difference to equal an integer number of cycles.

A suitable carrier-phase processing scheme must independently keep track of the fractional part of the nominal intermediate-frequency phase signal that it differences with each tracked signal's $\beta^j(t_{\mathrm{RA}})$ time history when it computes the $\phi^j_{1A}(t_{\mathrm{RA}})$ time history. The following recursive algorithm achieves this goal:

1) Initialize the fractional part of a common nominal intermediate-frequency phase signal to $\delta\eta_0 = 0$ at receiver clock time $t_{\mathrm{RA}0}$.

2) For all $k > 0$, update $\delta\eta_k$ and calculate the nominal number of completed whole cycles since the last sample $\Delta\eta_k$ by using the following recursive formulas:

$$\Delta\eta_k = \mathrm{floor}[f_{\mathrm{if}}(t_{\mathrm{RA}k} - t_{\mathrm{RA}(k-1)}) + \delta\eta_{k-1}] \quad (31a)$$

$$\delta\eta_k = [f_{\mathrm{if}}(t_{\mathrm{RA}k} - t_{\mathrm{RA}(k-1)}) + \delta\eta_{k-1}] - \Delta\eta_k \quad (31b)$$

This recursion keeps track of the nominal intermediate beat carrier phase $\eta(t_{\mathrm{RA}}) = \eta_0 + f_{\mathrm{if}}t_{\mathrm{RA}}$ in incremental format similar to how the outputs of Eqs. (28a) and (28b) keep track of $\beta^j(t_{\mathrm{RA}})$.

3) Initiate tracking of satellite j at receiver clock time $t_{\mathrm{RA}k_j}$ and set $\phi^j_{1A}(t_{\mathrm{RA}k_j}) = \delta\beta^j_{k_j} - \delta\eta_{k_j}$.

4) At each sample time $t_{\mathrm{RA}k} > t_{\mathrm{RA}k_j}$, compute $\phi^j_{1A}(t_{\mathrm{RA}k})$ using the recursive formula:

$$\phi^j_{1A}(t_{\mathrm{RA}k}) = \phi^j_{1A}(t_{\mathrm{RA}(k-1)}) + \left[\Delta\beta^j_k + \delta\beta^j_k - \delta\beta^j_{k-1}\right] - [\Delta\eta_k + \delta\eta_k - \delta\eta_{k-1}] \quad (32)$$

Note that it may be advantageous from a computational standpoint to keep track of $\phi^j_{1A}(t_{\mathrm{RA}k})$ as an integer part and a fractional part similar to how the increments to β and η are treated.

This algorithm is similar to the first one. In fact, the recursion in Eq. (32) works out to be identical to that of Eq. (29). This algorithm's key improvement is its use of $\delta\eta_{k_j}$ in its modified initialization of $\phi^j_{1A}(t_{\mathrm{RA}k_j})$. A tedious analysis shows that this new initialization yields the following initial difference between the nominal carrier-phase signals for GPS satellites i and j:

$$\gamma^i_{10A} - \gamma^j_{10A} = \mathrm{floor}[(f_{L1} + f_{\mathrm{if}})t_{\mathrm{RA}k_j} + \alpha_0 - \psi^j_{1A}(t_{\mathrm{RA}k_j})] - \mathrm{floor}[f_{\mathrm{if}}(t_{\mathrm{RA}k_j} - t_{\mathrm{RA}0})] - \mathrm{floor}[(f_{L1} + f_{\mathrm{if}})t_{\mathrm{RA}k_i} + \alpha_0 - \psi^i_{1A}(t_{\mathrm{RA}k_i})] + \mathrm{floor}[f_{\mathrm{if}}(t_{\mathrm{RA}k_i} - t_{\mathrm{RA}0})] \quad (33)$$

The floor[] functions on the right-hand side of this equation guarantee that this difference is an integer. Therefore, a receiver that uses this carrier-phase processing method is suitable for use with CDGPS algorithms that resolve double-differenced ambiguities exactly as integers.

This carrier-phase processing algorithm has been applied to an actual receiver. The receiver's original design used the carrier-phase initializations and updates in the first listed steps 1 and 2, and its carrier-phase outputs could not be used to implement CDGPS relative position determination calculations using double-differenced integer ambiguities. The receiver design has been modified to perform its carrier-phase initializations and updates using the new steps 1–4. The modified receiver has been used to perform double-differenced CDGPS relative position determination. Its outputs have been used to achieve rapid resolution of double-differenced ambiguities as integers and to verify subcentimeter relative position accuracies when operating on actual GPS data from terrestrial receivers.

C. Special Considerations for Dual-Frequency Carrier-Phase Processing

A dual-frequency receiver has very few requirements beyond the stipulation that the L2 carrier-phase processing must work like the L1 processing defined in the preceding subsection. In addition, the synthesizer for the L2 RF front-end's mixing signals must be driven by the same oscillator that drives the L1 RF front-end's mixing signals, and the sample clock for the digitized outputs of the L2 RF front-end must be synchronized with the L1 sample clock. These features ensure that the receiver time base is the same for both channels. This equivalence improves the accuracy of dual-frequency CDGPS estimation techniques because it avoids the need to estimate a second unknown receiver clock error.

D. Receiver Time Corrections

Some receivers correct their clocks based on the code-phase solution and report data using these corrected time tags. If this is done, then the reported pseudoranges and beat carrier phases also need to be corrected. The correction formulas that must be used are

$$(t_{\mathrm{RA}})_{\mathrm{corrected}} = (t_{\mathrm{RA}})_{\mathrm{raw}} - \delta t_{\mathrm{RAcode}} \quad (34a)$$

$$(\phi^j_{1A})_{\mathrm{corrected}} = (\phi^j_{1A})_{\mathrm{raw}} - f_{L1}\delta t_{\mathrm{RAcode}} \quad (34b)$$

$$(P^j_{1A})_{\mathrm{corrected}} = (P^j_{1A})_{\mathrm{raw}} - c\delta t_{\mathrm{RAcode}} \quad (34c)$$

V. Offline Simulation of GPS Carrier-Phase Measurements

The general idea of doing offline carrier-phase measurement simulation is not a new contribution, but this section's explanation of the details of how to implement a high-fidelity carrier-phase simulation does constitute a new contribution. It may be possible to study CDGPS systems using a simpler simulation, but the present development is based on the philosophy of making as few assumptions as possible. This philosophy avoids the possibility of leaving out some important effect which could have negative implications for a CDGPS system that is being evaluated based on the simulated data.

This section explains how to use the carrier-phase model of Sec. II to create simulated time histories of various quantities that are relevant to the evaluation of CDGPS estimation algorithms. These quantities include the positions of J GPS satellites, $\boldsymbol{r}^j(t)$ for $j = 1, \ldots, J$, the positions of two user receivers that also orbit on satellites, $\boldsymbol{r}_A(t)$ and $\boldsymbol{r}_B(t)$, the clock errors of the two receivers, $\delta t_{\mathrm{RA}}(t)$ and $\delta t_{\mathrm{RB}}(t)$, the ionospheric total electron content along each LOS path, $\mathrm{TEC}^j_A(t)$ and $\mathrm{TEC}^j_B(t)$ for $j = 1, \ldots, J$, the L1 and L2 carrier-phase measurements $\phi^j_{1A}(t_{\mathrm{RA}})$, $\phi^j_{1B}(t_{\mathrm{RB}})$, $\phi^j_{2A}(t_{\mathrm{RA}})$, and $\phi^j_{2B}(t_{\mathrm{RB}})$ for $j = 1, \ldots, J$, and the L1 and L2 pseudorange measurements $P^j_{1A}(t_{\mathrm{RA}})$, $P^j_{1B}(t_{\mathrm{RB}})$, $P^j_{2A}(t_{\mathrm{RA}})$, and $P^j_{2B}(t_{\mathrm{RB}})$ for $j = 1, \ldots, J$. Additional realism is modeled by including residual errors of the satellite clocks beyond those defined in Eq. (2) and ephemeris errors in the reported values of the GPS satellite positions. The measurement models include the ionospheric errors, the circular polarization windup errors, the carrier-phase multipath and thermal noise errors, the pseudorange thermal noise errors, and the line biases. Methods for computing these quantities are described in detail in the remaining subsections.

A. Clock Error Models

The simulation uses receiver-clock-error models and GPS satellite-clock-error models. The receiver-clock-error models are double-integrators that are driven by two white-noise terms. The receiver A model is [20]

$$\begin{bmatrix} \delta t_{\mathrm{RA}(k+1)} \\ \delta f_{\mathrm{RA}(k+1)} \end{bmatrix} = \begin{bmatrix} 1 & \Delta t_k \\ 0 & 1 \end{bmatrix} \begin{bmatrix} \delta t_{\mathrm{RA}k} \\ \delta f_{\mathrm{RA}k} \end{bmatrix} + \begin{bmatrix} \sqrt{S_f \Delta t_k + S_g \Delta t_k^3/12} & \sqrt{S_g \Delta t_k^3/4} \\ 0 & \sqrt{S_g \Delta t_k} \end{bmatrix} \boldsymbol{w}_{Ak} \tag{35}$$

where $\Delta t_k = t_{k+1} - t_k$ is the interval between the true GPS times $t_k (= t_{\mathrm{RA}k} - \delta t_{\mathrm{RA}k})$ and $t_{k+1} (= t_{\mathrm{RA}(k+1)} - \delta t_{\mathrm{RA}(k+1)})$, and where $\boldsymbol{w}_{Ak}$ is a two-dimensional Gaussian discrete-time white-noise process with a mean of zero and a covariance equal to the identity matrix. Appropriate values for the clock's phase drift intensity S_f and frequency drift intensity S_g for various oscillator types can be found in [20]. The clock error model of receiver B has the same form, though it may involve different drift intensities.

The simulated GPS satellite-clock-error models are defined by small differences between the actual values of a_{f0}^j and a_{f1}^j and the reported values in the navigation message. The actual values get used in Eqs. (13) and (15) to compute the simulated carrier phase and pseudorange measurements. The reported values get used by the CDGPS algorithm that is being studied. The discrepancies are chosen to reflect typical differences seen between broadcast corrections and after-the-fact corrections that are published with the precise GPS ephemerides.

B. Position Time Histories of the GPS Transmitters and User Receivers

The simulated GPS spacecraft position time histories $\boldsymbol{r}^j(t)$ for $j = 1, \ldots, J$ are generated by using almanac data, standard GPS orbit propagation algorithms, and perturbations. Almanac data have been used from YUMA Almanacs[‡], and the nominal GPS spacecraft positions have been calculated using the orbital models given in [15].

A perturbation is included for the antenna phase-center offset from the GPS satellite's center of mass, as in [11]. This latter perturbation is about a meter or less and is linked to the attitude of the GPS spacecraft relative to the Earth and the sun. The attitude is assumed to be nadir-pointing, but with small perturbations. These include constant perturbations and periodic librations with frequencies equal to multiples of the orbital frequency and with the highest multiple being three. These perturbations are sized to be consistent with the reported attitude dynamics of the GPS spacecraft.

The simulation models ephemeris errors by reporting erroneous GPS spacecraft positions for use by the CDGPS algorithm that is being studied. These errors take the form of differences between the reported positions and the actual positions used to generate the carrier-phase and pseudorange measurements in Eqs. (13) and (15). The ephemeris errors are modeled by three independent four-term Fourier series, one each for the along-track, cross-track, and altitude errors. Each series includes constant terms and once-, twice-, and thrice-per-orbit oscillations. The Fourier coefficients are chosen randomly, and their magnitudes are scaled to be consistent with typical differences between the broadcast GPS ephemerides and the precise ephemerides that are computed after the fact.

The position time histories of user receivers A and B are propagated by numerically integrating orbital dynamics differential equations as in [12]. These differential equations include a 30×30 Earth gravity model and the effects of solar radiation pressure and atmospheric drag.

[‡]YUMA Almanacs, http://www.navcen.uscg.gov/ftp/GPS/almanacs/yuma/, Jan. 2005.

C. Simulation of the Ionosphere

The simulation of $\mathrm{TEC}_A^j(t)$ and $\mathrm{TEC}_B^j(t)$ uses the ionosphere model of [12]. It is a modified form of the standard ionosphere model that gets broadcast with the GPS navigation data message [15]. The modification incorporates altitude dependence into the electron density model. The altitude dependence is approximated by two altitude regions with two different exponential scale heights. The simulation computes TEC values by numerically integrating the modeled electron densities along LOS vectors. The numerical integration is based on piecewise exponential models and works with interpolated natural logarithms of the electron densities.

D. Iterative Calculation of Transmission Times

The signal transmission time $\delta t_{\mathrm{trn}A}^j$ that is defined by Eq. (4) must be calculated iteratively because it appears on both sides of the equation. The transmission delay calculation starts with a known true GPS time of reception at the antenna $t - \delta t_{\ell_n A}$. This true time is used to compute the receiver position at the reception time $\boldsymbol{r}_A(t - \delta t_{\ell_n A})$. The iterative $\delta t_{\mathrm{trn}A}^j$ calculation starts with the guess $\delta t_{\mathrm{trn}A}^j = \delta t_{\ell_n A}$, which it substitutes into the right-hand side of Eq. (4) to compute an updated $\delta t_{\mathrm{trn}A}^j$. This update is then resubstituted into the right-hand side of Eq. (4) to improve the estimate of $\delta t_{\mathrm{trn}A}^j$. This process repeats until the updates to $\delta t_{\mathrm{trn}A}^j$ are very small compared with the time of a carrier cycle $1/f_{L1}$. The convergence of this procedure can be hastened by using a Newton–Raphson solution procedure for $\delta t_{\mathrm{trn}A}^j$ in place of the ad hoc iteration defined here.

The iteration must update the $\delta t_{\mathrm{ion}A}^j$ ionospheric delay term in Eq. (4) each time $\delta t_{\mathrm{trn}A}^j$ changes. This is necessary because the LOS path of the TEC numerical integration is a function of $\boldsymbol{r}^j(t - \delta t_{\mathrm{trn}A}^j)$.

E. Multipath Error Model

Carrier-phase multipath errors such as $\delta\phi_{\mathrm{mp1}A}^j$ and $\delta\phi_{\mathrm{mp2}A}^j$ are modeled as being functions of the direction of the LOS vector in the body coordinate system of the user satellite. The user satellite attitude is assumed to be nadir-pointing, possibly with small perturbations that include constant biases and librations at multiples of the orbital period. The highest multiple that may be included is four librations per orbit. The multipath error is modeled by a spherical harmonic expansion in the satellite-relative azimuth and elevation of the received LOS vector. Figure 3 depicts the azimuth and elevation dependence of an example multipath error model by mapping the carrier-phase error into a shading that depends on the direction of the received signal. Independent models of this form are used for the L1 and L2 frequencies. The maximum multipath phase error for each carrier frequency is on the order of $(0.005\ \mathrm{m})/\lambda$.

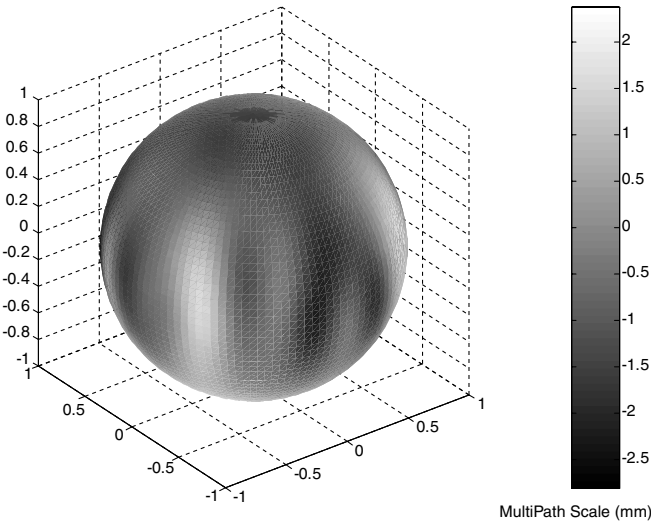

Fig. 3 Azimuth and elevation dependence of an example carrier-phase multipath error model.

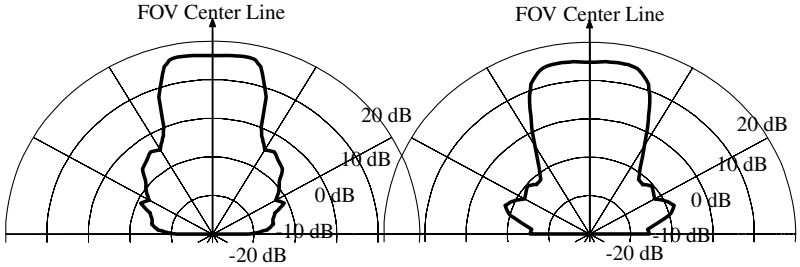

Fig. 4 Cross sections of axisymmetric GPS transmission gain patterns used in the simulation.

F. Signal Availability and Receiver Thermal Noise Model

The signal availability and the measurement errors caused by receiver thermal noise both depend on antenna gain patterns and geometry. If the Earth occults the LOS, then the signal is not available. If the signal is not occulted, then the receiver and transmitter gain patterns and the free-space gain are used to compute the received signal's power, and this power level and the receiver noise level are used to compute the carrier-to-noise ratio C/N_0. If C/N_0 is too low for acquisition and tracking, then the signal is deemed to be unavailable. If the signal is not occulted and if C/N_0 is high enough, then carrier-phase and pseudorange measurements are computed by the simulation. The value of C/N_0 and the receiver design parameters B_{PLL}, B_{DLL}, t_{acc}, and t_{eml} determine the thermal measurement noise standard deviations in Eqs. (9) and (16). The simulated values for B_{PLL}, B_{DLL}, t_{acc}, and t_{eml} and for the minimum usable C/N_0 are chosen to be appropriate for an orbital user receiver that is equipped to processes weak signals. The simulation uses the standard deviations from Eqs. (9) and (16) and a Gaussian random number generator to simulate actual thermal noise errors for the carrier-phase and pseudorange measurements in Eqs. (13) and (15).

Accurate computation of the received C/N_0 and the corresponding signal availability is critical to correct simulation of CDGPS performance in HEO and GEO. This is true because few strong signals are available in these altitude regimes. Several factors go into this computation. Orbital and attitude geometry for the GPS transmitter spacecraft and the user spacecraft provide the distance between the transmitter and receiver and the LOS directions in the coordinate systems of the transmitter and receiver antennas. The LOS directions and the antenna gain patterns are used to determine the antenna gains. The transmitter gain patterns include models of the antenna side lobes because most of the available signals in the GEO to HEO altitude regime are side-lobe signals. Cross sections of the simulated L1 and L2 transmitter gain patterns are shown in Fig. 4. Receiver gain patterns are modeled similarly, but their actual forms are a function of the type of antenna used. The transmitter gain, the receiver gain, the free-space gain due to the distance between the receiver and the transmitter, and the effective isotropic radiated power (EIRP) are used to compute the received power C. Typical receiver thermal noise levels and noise figures are then used to compute the received noise power spectral density N_0, and this completes the information needed to compute C/N_0 for use in calculating signal availability and the carrier-phase and pseudorange thermal noise standard deviations.

G. Circular Polarization Windup Model

The carrier-phase errors due to circular polarization windup, $\delta\phi^j_{\mathrm{pwu}A}$ and $\delta\phi^j_{\mathrm{pwu}B}$, are modeled using Eqs. (7), (8a), and (8b). The orbital and attitude geometric quantities needed for this model are available as byproducts of the calculations of ephemeris errors, multipath errors, and C/N_0 levels.

H. Simulated Carrier-Phase and Pseudorange Measurements

The carrier-phase and pseudorange measurement models are simple evaluations of Eqs. (13) and (15). These evaluations use the truth positions, transmission delays, and ionospheric TEC values along with the error terms that are computed using the previously described models. These calculations use reasonable fixed values for the receiver line biases $\delta t_{\ell_{\mathrm{n}}\,1A}$, $\delta t_{\ell_{\mathrm{n}}\,2A}$, $\delta t_{\ell_{\mathrm{n}}\,1B}$, and $\delta t_{\ell_{\mathrm{n}}\,2B}$.

The simulation generates measurements only for the GPS satellites that have sufficiently high C/N_0. If there are too many signals for the presumed number of channels (nominally 12), then the receiver gives priority first to signals that are already being tracked. New signals are tracked when a channel becomes available, and the receiver decides between multiple possible new signals for a given available channel based on one of two priority schemes. The first scheme gives the highest priority to the signal with the highest received C/N_0 on the L1 frequency. The second scheme gives the highest priority to the available GPS satellite with the highest elevation as measured relative to the receiving antenna's FOV.

VI. Carrier-Phase Simulation Results

The simulation has been tested by using it as a tool for evaluating the CDGPS relative spacecraft position estimation algorithms of [13,14]. Three of the simulations have considered short- and long-baseline single-frequency CDGPS in LEO and short-baseline, single-frequency and dual-frequency CDGPS in GEO. Results from these cases are discussed next.

A. Short-Baseline LEO Case

The short-baseline LEO case shows reasonable performance. It considers a pair of user spacecraft separated by 2 km in an average orbit with an apogee altitude of 580 km, a perigee altitude of 560 km, and an inclination of 28 deg. The satellites both carry patch antennas with hemispherical gain patterns that point nominally in the zenith direction, and the satellites' attitudes can undergo librations of as much as 4 deg about any one axis.

Seven L1 GPS signals are tracked by both receivers during one 300 s portion of the orbit. Their C/N_0 values range from 46.5 to 55.4 dB · Hz over this data span, and they produce a geometric dilution of precision (GDOP) of two.

The simulation's L1 carrier-phase and pseudorange measurements have been processed by the CDGPS estimation algorithm of [13] to produce the relative spacecraft position estimates whose errors from the simulation's truth model are shown in Fig. 5. These errors are consistent with the results shown in [13] for a similar case that uses a hardware-in-the-loop signal simulator and data from an actual space-qualified GPS receiver. In both cases, the CDGPS algorithm is able to resolve the double-differenced integer ambiguities correctly in a single measurement sample, and the relative navigation errors are less than 5 mm. The errors for the offline simulation are about 2–5 times smaller than those for the hardware-in-the-loop simulation of [13]. This difference may be due to the higher C/N_0 values experienced in the offline simulation scenario.

The single-differenced circular polarization windup errors, $\delta\phi^j_{\mathrm{pwu}A} - \delta\phi^j_{\mathrm{pwu}B}$, do not play an important role in this case. They never exceed 1.6 deg of carrier phase, which translates into 0.0008 m of differential range error.

B. Long-Baseline LEO Case

A long-baseline LEO case has been run to evaluate the impact of significant ionospheric variations, carrier-phase windup errors, and

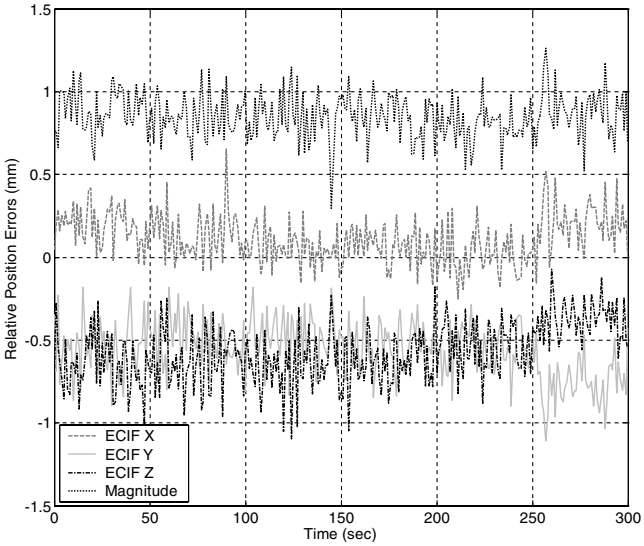

Fig. 5 Relative-position-error time histories of [13] CDGPS algorithm applied to simulated LEO data with a 2 km baseline between user satellites A and B.

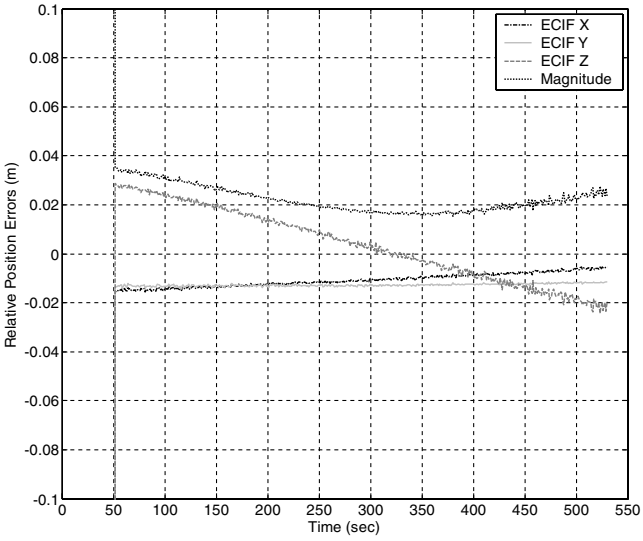

Fig. 6 Relative-position-error time histories of [13] CDGPS algorithm applied to simulated LEO data with a 100 km baseline.

ephemeris errors on a single-frequency L1 CDGPS algorithm. The two satellites are separated by 100 km in this case, and their average orbit has an apogee altitude of 660 km, a perigee altitude of 645 km, and an inclination of 87.1 deg. There are seven GPS satellites that are tracked by both receivers during one 530 s portion of their orbits. These satellites produce GDOP values that range from 2.3 to 2.5, and their range of C/N_0 values is similar to the short-baseline LEO case.

Figure 6 plots the CDGPS relative navigation errors for this scenario when using the algorithm of [13]. This figure demonstrates that the long-baseline CDGPS performance deteriorates in two ways. First, the algorithm requires more time to correctly resolve the double-differenced integer ambiguities, 50 s in the long-baseline case vs a single sample for the short-baseline case. The relative position errors are on the order of 1 m before $t = 50$ s, but they decrease to be on the order of 0.03 m or less after the integers have been correctly resolved. The long-baseline errors never approach the 0.001 m accuracy level of the short-baseline case.

The poorer performance of the long-baseline case is caused in part by the ionospheric and circular polarization errors. The maximum single-differenced ionospheric error yields 0.005 m of differential range error for this case, and the maximum single-differenced circular polarization windup error yields 0.002 m of differential range error. These significant systematic errors cause part of the degradation of accuracy in Fig. 6 as compared to Fig. 5. In addition, GPS satellite ephemeris errors contribute as much as 0.005 m of differential range error. The exact impact of each error source on the final differential solution accuracy has not been isolated for this case, but such an analysis could be performed using the simulation's truth model data, and it could shed light on how best to improve accuracy over long baselines.

Results for a dual-frequency estimator operating on long-baseline data from this paper's simulator are presented in [14]. Simulated results in [14] are compared with long-baseline dual-frequency estimator results in [21] that use actual data from the GRACE mission. The similarities noted in [14] between the two sets of results provide evidence that the simulation is realistic.

C. GEO Case

Single-frequency and dual-frequency GEO cases with a short 3 km baseline have been tested to determine whether CDGPS techniques are feasible in this altitude regime. The two principal questions are whether enough satellites are available with sufficient signal strength and whether the available satellites allow resolution of double-differenced carrier-phase ambiguities. The simulation assumes that each GEO spacecraft carries a patch antenna with a hemispherical gain pattern, that the L1 signal can be acquired and tracked down to $C/N_0 = 18$ dB · Hz, and that the L2 acquisition and tracking threshold is $C/N_0 = 15$ dB · Hz. This is reasonable given the results of [6–8]. The simulation produces measurements from 11 or 12 commonly visible GPS satellites at all times because the assumed weak-signal tracking capabilities of the receiver enable it to use side-lobe signals. The value of GDOP ranges from 7.6 to 13.2 in this scenario; it is high due to the poor geometry of the available satellites.

The along-track (A-T), cross-track (C-T), and altitude (alt) relative navigation errors of three CDGPS algorithms are plotted for this case on the top three graphs of Fig. 7. GDOP and the number of GPS satellites that are tracked by both receivers, N_{sats}, are plotted on the lower graph of Fig. 7. The position error time histories denoted by the solid gray lines and those denoted by the black dash-dotted lines are both for the dual-frequency CDGPS algorithm of [14], but with two different values of a tuning parameter. The light gray dashed error time histories correspond to a signal-frequency L1 algorithm like that of [13]. These results indicate that the two [14] algorithms do very well in along-track and cross-track, achieving peak errors of less than 0.04 m, and reasonably well in altitude, with peak errors below 0.25 m. Their poorer performance in altitude is expected because the high GDOP values tend to affect altitude the most. The single-frequency algorithm has superior performance on all three axes; the respective peak along-track, cross-track, and altitude errors are 0.014, 0.008, and 0.090 m, except between $t = 5500$ and $t = 5750$ s. The large error spike that occurs during this interval is caused by the setting of a GPS satellite behind the Earth. Just before it sets, the differential TEC value between the two user receivers becomes large and causes the negative spike in the relative altitude error of the L1-only estimator. The two dual-frequency estimators do not produce error spikes because they estimate the differential TEC and correct for it.

The good performance of all three CDGPS algorithms, except when the L1-only algorithm produces the error spike, is the result of their ability to rapidly resolve the double-differenced carrier-phase ambiguities. Once the ambiguities have been resolved, the relative-position-error components should be on the order of GDOP times the carrier-phase measurement error. Given measurement errors on the order of 0.01 m and GDOP in the range of 7.6–13.2, one expects the relative navigation errors to be on the order of 0.076–0.132 m, and they are.

It is surprising that the carrier-phase ambiguities can be resolved exactly as integers in a short amount of time. The expected range of the steady-state relative position uncertainties between 0.076 and 0.132 m translates into a range of 0.40–0.70 carrier wavelengths at the L1 frequency and 0.31–0.54 wavelengths at L2. One might think that these numbers would translate directly into 1-σ L1 ambiguity uncertainties of 0.40–0.70 cycles and 1-σ L2 ambiguity uncertainties

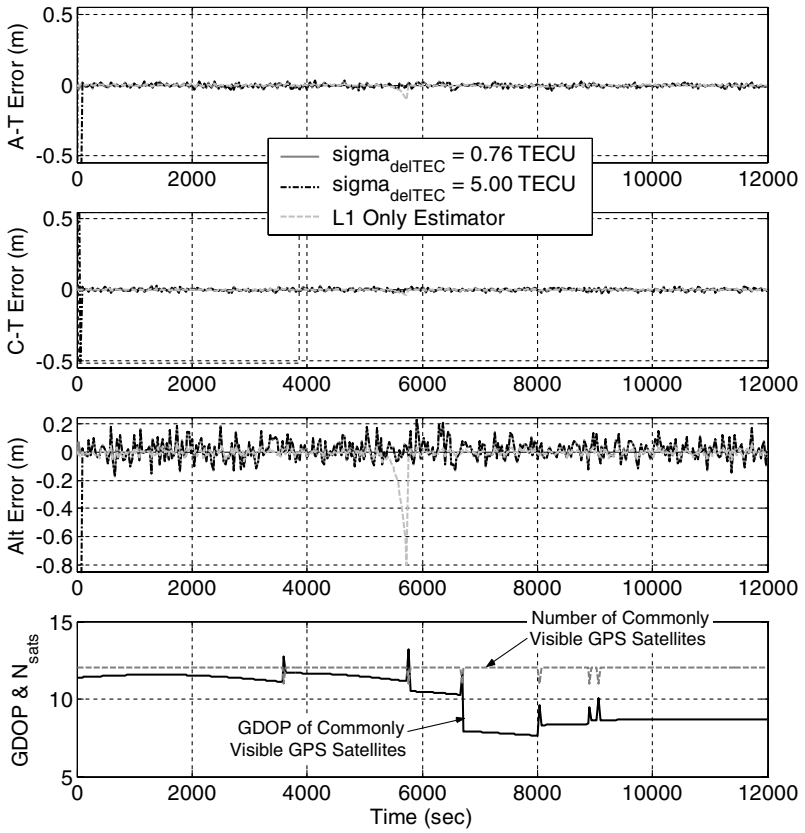

Fig. 7 Relative-position-error, GDOP, and N_{sats} time histories of [13,14] CDGPS algorithms applied to simulated GEO data with a 3 km baseline.

in the range of 0.31–0.54 cycles, which would render the ambiguities unresolvable as integers. Fortunately, the simulation is saying that the uncertainties are much smaller in the subspace of the estimation problem that is spanned by the integer ambiguities. This is why they can be resolved so quickly.

VII. Summary and Conclusions

This paper has developed mathematical models of GPS carrier-phase measurements and techniques for simulating them. The signal models and the simulation include such affects as receiver and transmitter clock errors, carrier-phase ambiguities, ionospheric errors, and errors due to multipath, thermal noise, line bias, and the GPS signal's circular polarization. Signal models and simulation techniques have been developed for the two GPS frequencies, L1 and L2.

Analysis of carrier-phase signals has been performed to determine when the carrier-phase ambiguities equal integer numbers of cycles. The ambiguities are integers only after double-differencing in most cases. The one exception is that single-differenced carrier phases can take on integer values if the two receivers use the same clock. This is normally the case when doing GPS-based attitude determination.

Analysis of the carrier-phase measurements has been used to develop guidelines for correct receiver carrier-phase measurement processing. Data from a receiver that complies with these guidelines can be used to resolve double-differenced integer ambiguities. Failure to comply leads to an inability to resolve the ambiguities as integers.

Simulation results in conjunction with CDGPS algorithms demonstrate the efficacy and limitations of CDGPS techniques in scenarios ranging from LEO to GEO. LEO relative position estimation can be performed to subcentimeter accuracy if the two spacecraft are separated by about a kilometer, and double-differenced integer ambiguities can be resolved almost instantaneously. If the separation of two LEO user spacecraft is on the order of 100 km, then ambiguity resolution can be slowed, and systematic ionospheric errors, carrier-phase polarization errors, and ephemeris errors can cause the relative position errors to degrade to the order of several centimeters. CDGPS techniques with integer ambiguity resolution are possible in GEO if the user receivers can track L1 signals as weak as 18 dB · Hz, L2 signals as weak as 15 dB · Hz, or both. Relative position accuracies better than 0.25 m can be achieved in GEO over baselines on the order of several kilometers.

Acknowledgments

This work has been supported in part by NASA Goddard Space Flight Center through cooperative agreement No. NCC5-722, with Michael Moreau as the agreement monitor, and through a NASA Graduate Student Researcher Program Fellowship, with Russell Carpenter as the fellowship monitor.

References

[1] Leitner, J., Bauer, F., Folta, D., Carpenter, R., Moreau, M., and How, J., "Formation Flight in Space," *GPS World*, Vol. 13, No. 2, Feb. 2002, pp. 22–31.

[2] Busse, F. D., How, J. P., and Simpson, J., "Demonstration of Adaptive Extended Kalman Filter for Low-Earth-Orbit Formation Estimation Using CDGPS," *Journal of Navigation*, Vol. 50, No. 2, 2003, pp. 79–93.

[3] Ebinuma, T., Bishop, R. H., and Lightsey, E. G., "Integrated Hardware Investigations of Precision Spacecraft Rendezvous Using the Global Positioning System," *Journal of Guidance, Control, and Dynamics*, Vol. 26, No. 3, May–June 2003, pp. 425–433.

[4] Leung, S., and Montenbruck, O., "Real-Time Navigation of Formation-Flying Spacecraft Using Global-Positioning-System Measurements," *Journal of Guidance, Control, and Dynamics*, Vol. 28, No. 2, March–April 2005, pp. 226–235.

[5] Wolfe, J. D., and Speyer, J. L., "Effective Estimation of Relative Positions in Orbit Using Differential Carrier-Phase GPS," *Proceedings of the AIAA Guidance, Navigation, and Control Conference*, AIAA Paper 2004-4777, 2004.

[6] Psiaki, M. L., "Block Acquisition of Weak GPS Signals in a Software Receiver,"*Proceedings of the ION GPS 2001*, Inst. of Navigation, Fairfax, VA, 2001, pp. 2838–2850.

[7] Psiaki, M. L., and Jung, H., "Extended Kalman Filter Methods for

Tracking Weak GPS Signals," *Proceedings of the ION GPS 2002*, Inst. of Navigation, Fairfax, VA, 2002, pp. 2539–2553.

[8] Psiaki, M. L., "FFT-Based Acquisition of GPS L2 Civilian CM and CL Signals," *Proceedings of the ION GNSS 2004*, Inst. of Navigation, Fairfax, VA, 2004, pp. 457–473.

[9] Goad, C., "Surveying with the Global Positioning System," *Global Positioning System: Theory and Applications*, Vol. 2, edited by Parkinson, B. W., and Spilker, J. J., Jr., AIAA, Washington, D.C., 1996, pp. 501–517.

[10] Teunissen, P. J. G., and Kleusberg, A., "GPS Observation Equations and Positioning Concepts," *GPS for Geodesy*, 2nd ed., edited by Teunissen. P. J. G., and Kleusberg, A., Springer, New York, 1998, pp. 187–229.

[11] Leick, A., *GPS Satellite Surveying*, 3rd ed., Wiley, New York, 2004, pp. 170–187, 228–300.

[12] Psiaki, M. L., "Satellite Orbit Determination Using a Single-Channel Global Positioning System Receiver," *Journal of Guidance, Control, and Dynamics*, Vol. 25, No. 1, Jan.–Feb. 2002, pp. 137–144.

[13] Mohiuddin, S., and Psiaki, M. L., "Satellite Relative Navigation Using Carrier-Phase Differential GPS with Integer Ambiguities," *Journal of Guidance, Control, and Dynamics* (to be published), 2007.

[14] Psiaki, M. L., and Mohiuddin, S., "Relative Navigation of High-Altitude Spacecraft Using Dual-Frequency Civilian CDGPS," *Proceedings of the ION GNSS 2005*, Inst. of Navigation, Fairfax, VA, 2005, pp. 1191–1207.

[15] Anon., "Navstar GPS Space Segment/Navigation User Interfaces," ARINC Research Corp. ICD-GPS-200, Rev. C, 14 Jan. 2003, El Segundo, CA, pp. 86–100.

[16] Klobuchar, J. A., "Ionospheric Effects on GPS," *Global Positioning System: Theory and Applications*, Vol. 1, edited by Parkinson, B. W., and Spilker, J. J., Jr., AIAA, Reston, VA, 1996, pp. 485–515.

[17] Lightsey, E. G., and Parkinson, B. W., "GPS Based Attitude Determination on Nonaligned Antenna Arrays," *Proceedings of the ION GPS 1996*, Inst. of Navigation, Fairfax, VA, Sept. 1996, pp. 1081–1090.

[18] Lightsey, E. G., "Spacecraft Attitude Control Using GPS Carrier Phase," *Global Positioning System: Theory and Applications*, Vol. 2, edited by Parkinson, B. W., and Spilker, J. J., Jr., AIAA, Reston, VA, 1996, pp. 461–480.

[19] Van Dierendonck, A. J., "GPS Receivers," *Global Positioning System: Theory and Applications*, Vol. 1, edited by Parkinson, B. W., and Spilker, J. J., Jr., AIAA, Reston, VA, 1996, pp. 329–407.

[20] Brown, R. G., and Hwang, P. Y. C., *Introduction to Random Signals and Applied Kalman Filtering*, 3rd ed., Wiley, New York, 1997, pp. 428–432.

[21] Kroes, R., Montenbruck, O., Bertiger, W., and Visser, P., "Precise GRACE Baseline Determination Using GPS," *GPS Solutions*, Vol. 9, No. 1, April 2005, pp. 21–31.